Atmos. Chem. Phys., 23, 13819–13834, 2023
https://doi.org/10.5194/acp-23-13819-2023

Atmospheric Chemistry and Physics
Open Access
EGU

Aircraft ice-nucleating particle and aerosol composition measurements in the western North American Arctic

Alberto Sanchez-Marroquin, Sarah L. Barr, Ian T. Burke, James B. McQuaid, and Benjamin J. Murray

School of Earth and Environment, University of Leeds, Woodhouse Lane, Leeds, LS2 9JT, UK

Correspondence: Benjamin J. Murray (b.j.murray@leeds.ac.uk)

Received: 18 August 2022 – Discussion started: 20 September 2022
Revised: 15 August 2023 – Accepted: 21 August 2023 – Published: 7 November 2023

Abstract. Knowledge of the temperature-dependent concentration of ice-nucleating particles (INPs) is crucial to understanding the properties of mixed-phase clouds. However, the sources, transport and removal of INPs around the globe, and particularly in the Arctic region, are poorly understood. In the Arctic winter and spring, when many local sources are covered by ice and snow, it is not clear which INP types are important. In this study, we present a new dataset of aircraft-based immersion mode INP measurements and aerosol size-resolved composition in the western North American Arctic from 11 to 21 March 2018. Aerosol samples were collected between $\sim$70 and 600 m above the surface on filters that were analysed using both a freezing droplet-based assay and scanning electron microscopy with energy dispersive spectroscopy (SEM-EDS). The measured INP concentrations were at or close to the limit of detection, with concentrations at $-20\,^{\circ}\mathrm{C}$ of $1\,\mathrm{L}^{-1}$ or below. The size-resolved composition measurements indicates that the aerosol concentrations were low, dominated mostly by sea spray aerosol and mineral dust. Further analysis shows that mineral dust is important for the ice-nucleating properties of our samples, dominating over the sea spray aerosol particles in the four cases we analysed, suggesting that mineral dust is a relevant type of INP in the Alaskan springtime Arctic. Furthermore, the INP concentrations are more consistent with fertile soil dusts that have an ice-active biological component than what would be expected for the ice-active mineral K-feldspar alone. While we cannot rule out local high-latitude sources of dust, the relatively small size of the mineral dust implies that the dust was from distant sources.

1 Introduction

Clouds containing both supercooled liquid water and ice are known as mixed-phase clouds, and they reflect a substantial amount of the incoming solar shortwave radiation that reaches the Earth (Boucher, 2013). The lifetime, as well as the amount of radiation that these clouds reflect, is strongly affected by the partitioning between liquid and ice (Storelvmo et al., 2015). When above temperatures required for homogeneous freezing (below $\sim -35\,^{\circ}\mathrm{C}$), ice formation in mixed-phase clouds is initiated by the presence of a small fraction of the aerosol particles known as ice-nucleating particles (INPs) (Murray et al., 2012). Once ice crystals nucleate, they can grow more rapidly than liquid cloud droplets since ice has a lower equilibrium vapour pressure than supercooled water. This process can lead to the precipitation of the ice crystals, removing liquid water from a cloud (Korolev et al., 2017; Vergara-Temprado et al., 2018; Hawker et al., 2021). Ice-related processes in mixed-phase clouds such as the primary production of ice and the link to INP concentration are commonly oversimplified in climate models, which contributes to large discrepancies in the amount of water and ice that the models simulate (Komurcu et al., 2014; McCoy et al., 2016, 2018). The difficulty of properly representing the current water and ice mixing state of these clouds is responsible for the large uncertainty of the cloud-phase feedback (Storelvmo et al., 2015).

As the atmosphere warms, mixed-phase clouds will contain more supercooled water, leading to a reduction in shortwave radiation reaching the surface but also a decrease the outgoing longwave radiation flux (Ceppi et al., 2017; Murray et al., 2021). Hence, mixed-phase mid- to high-latitude

clouds over the ocean have a negative feedback (Tan et al., 2016), whereas clouds over high-albedo ice or snow-covered surfaces have a positive feedback (Tan et al., 2016). The strength of these feedbacks depends on the balance between ice and supercooled water in these clouds both in the present and future climate. Hence, better understanding the sources and concentrations of atmospheric INPs, particularly at the mid- to high-latitudes, could help to reduce the uncertainty associated with cloud feedbacks.

Only a small fraction of aerosol particles have the potential to become INPs. Transported dust from the deserts is one of the most important sources of worldwide atmospheric INPs, especially at temperatures below −15 °C (Hoose and Mohler, 2012; Vergara-Temprado et al., 2017; Kanji et al., 2017). Given the fact that substantial amounts of dust are transported from the deserts to the Arctic (Fan, 2013; Huang et al., 2015; Francis et al., 2018), this dust could contribute to the INP population of the region (Irish et al., 2019; Yun et al., 2022). Additionally, local sources of high-latitude dust are known to contribute to the dust budget in the Arctic (Bullard et al., 2016; Groot Zwaaftink et al., 2016; Meinander et al., 2022; Shi et al., 2022). Some of these sources of high-latitude dust have been found to contribute to the Arctic INP population (Tobo et al., 2019; Sanchez-Marroquin et al., 2020; Si et al., 2019). A fraction of the INPs in the Arctic are also of biogenic origin (Wex et al., 2019; Porter et al., 2022), some of which may be associated with biogenic material in sea spray, and some of which may be from terrestrial sources (Wilson et al., 2015; DeMott et al., 2016; Vergara-Temprado et al., 2017; Irish et al., 2017; McCluskey et al., 2018; Bigg and Leck, 2001; Creamean et al., 2019, 2020; Hartmann et al., 2020). Biogenic material attached to dust particles could be an important part of these terrestrial INPs (O'Sullivan et al., 2014, 2015; Tobo et al., 2019). Other types of aerosol particles such as volcanic ash or biomass burning particles could also contribute to the INP population in the Arctic (Prenni et al., 2009).

The available literature data indicate that the INP concentrations in the Arctic are highly variable depending on the season and location (Murray et al., 2021). Using samples from land-based sites around the Arctic collected over several years, Wex et al. (2019) found that Arctic INP concentrations reach a minimum during winter, but they increase through spring and reach a maximum around the summer, suggesting that concentrations are highest when the transport of aerosol from the low latitudes is at its weakest (the summer). Similarly, year-round measurements in the central Arctic indicate peak concentrations in the summer months of 2020 (Creamean et al., 2022). Creamean et al. (2022) suggested that local Arctic marine sources might contribute to the elevated INP populations in the summer. Porter et al. (2022) also found elevated summertime INP concentration during August 2018 in the pack ice near the North Pole. However, in contrast to Creamean et al. (2022), Porter et al. (2022) concluded that these very active INPs were associated with air masses originating from lower-latitude ice-free regions along the Russian coast, whereas air masses that had spent the preceding week or so over ice-covered surfaces (in the central Arctic pack ice) had very low INP particle concentrations. The central Arctic in 2018 and 2020 appears to be rather different, with Porter et al. (2022) reporting up to $2\,L^{-1}$ at −15 °C in 2018, whereas Creamean et al. (2022) reported peak INP concentrations that were 2 orders of magnitude lower in 2020. Hence, there may simply be a great deal of variability, and the contrasting conclusions between Porter et al. (2022) and Creamean et al. (2022) may be appropriate for their respective study periods. Creamean et al. (2018) found a similar trend in INP concentrations to Wex et al. (2019) over spring, with coarse particles being responsible for the higher INP concentration event. However, a recent study did not find strong seasonality of Arctic INPs at Ny-Ålesund, although these measurements were limited to being between April and August 2018 (Rinaldi et al., 2021). Furthermore, there have been very few INP measurements from aircraft. Given there are strong aerosol sinks in the boundary layer, whereas the air above the boundary layer can be stratified with corresponding long aerosol lifetimes (Carslaw, 2022), vertical measurements are required. Hartmann et al. (2020) report INP spectra for late March and early April north of 80° over the Fram Strait and Arctic Ocean and report that the highest INP concentrations ($2 \times 10^{-2}\,L^{-1}$ at −15 °C) correspond to the boundary layer, indicating a local marine source even though the region was mostly ice covered. Overall, the picture of INP concentrations in the Arctic is that of high variability, both spatial and temporal (on daily to yearly timescales), with the potential for high variability in local sources, transport from lower latitudes, and local INP sinks.

In this paper, we present a set of immersion mode INP and aerosol size-resolved composition measurements carried out in the western North American Arctic during March 2018 using an aircraft. Our measurements were carried out at different altitudes up to ∼ 600 m above sea level both within and above the boundary layer. INP measurements were combined with aerosol characteristics determined using scanning electron microscopy with energy dispersive spectroscopy (SEM-EDS) to indicate the types of INPs that are were most important during this campaign.

2 Sampling location and methods

Aerosol particles were sampled from the UK's BAe-146 FAAM atmospheric research aircraft during the Measurements of Arctic Cloud, Snow and Sea Ice in the Marginal Ice ZonE (MACSSIMIZE) campaign, based in Fairbanks, Alaska (US), in March 2018. The majority of the measurements were carried out close to the northern coast of Alaska and the Canadian territory of Yukon, both over land and over the Arctic Ocean, as shown in Fig. 1, where the flight track

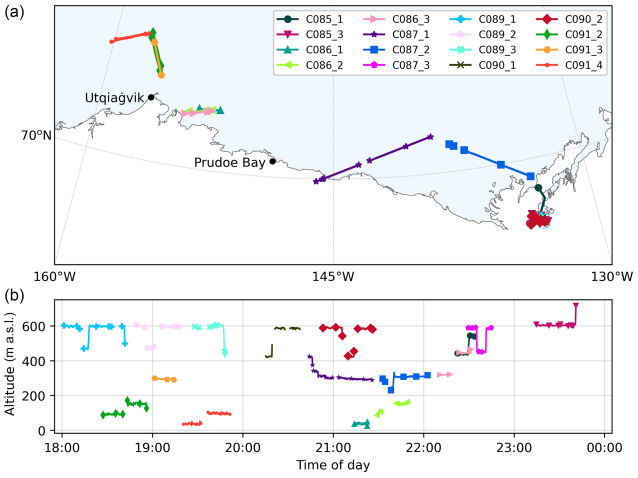

Figure 1. Flight tracks of the samples collected in this study and described in Table 1 **(a)**. GPS altitude at which the samples were collected **(b)**. The altitude is presented against the UTC time at which the samples were collected (although they were collected across several days).

corresponding to each sample has been presented. Measurements were carried out at altitudes between 40 and 600 m above sea level, as detailed in Table 1 along with other pertinent information. Some filters were collected in a single run on a constant heading and height, while others were collected over several runs, with the filters system mostly closed during turns between the runs and altitude changes, although this was not possible for all filters. Filters were collected over 9 to 36 min, which at the speed at which sampling takes place of $\sim 360\,\mathrm{km\,h^{-1}}$ corresponded to a horizontal distance of between ~ 50 and ~ 200 km. All the sampling was done outside of cloud and precipitation.

Aerosol particles were collected using the filter inlet system on board the FAAM BAe-146, which has been characterized by Sanchez-Marroquin et al. (2019). Briefly, this inlet is located outside the skin of the FAAM BAe-146 and brings aerosol particles to a filter located inside the cabin with a 45° angle bend. The sampling occurs in sub-isokinetic conditions, which enhances coarse-mode aerosol particles. Sampling efficiency for particles with diameters above 20 µm becomes very small due to inertial losses in the system (at the bend). No treatment (heat or drying) is applied to the sampled air mass, although the cabin was warmer than the ambient air in this campaign, and hence the RH of air passing through the inlet system once inside the aircraft is very low. The system allowed us to collect two aerosol samples in parallel: one on a polycarbonate filter (Whatman Nuclepore polycarbonate track-etched filters, 47 mm diameter with a pore size of 0.4 µm) and one on a Teflon filter (Sartorius polytetrafluoroethylene, 47 mm diameter with a pore size of 0.45 µm). For these filter types, the particle collection efficiency is likely to be close to 100 % for the relevant size ranges, as discussed in Sanchez-Marroquin et al. (2019) using the data of Soo et al. (2016) and Lindsley (2016).

The ice-nucleating particle assay was conducted in a temporary laboratory set up in a hotel room near the aircraft base in Fairbanks, Alaska, with minimum time between sampling and analysis. Most filters were analysed a matter of hours after collection; however, where this was not possible they were stored at $\sim -18\,^{\circ}\mathrm{C}$ for a few days prior to analysis. This approach has a number of advantages compared to the commonly used strategy of bringing filters back to a laboratory for latter analysis. Firstly, analysis of field blanks can reveal sources of contamination that can be reduced by making adjustments to the experimental protocol; secondly, we can try to adjust the sampling methodology (such as sampling time) to fit the INP concentration; and, thirdly, we can minimize storage and transport of filters, thus reducing potential biases. Teflon filters were used to perform a droplet-on-filter freezing assay to quantify the INP concentration, as described in detail in Price et al. (2018) and also used by Sanchez-Marroquin et al. (2020, 2021). The technique was first described by Schnell (1982), and our version of this assay makes use of the Asymptote EF600 Stirling cooler described in Whale et al. (2015). For the present study we pipetted 2 µL pure water droplets on top of each filter that had been exposed to aerosol particles (or handling blanks). On average, we pipetted 54 (with a standard deviation of 5) droplets per filter. The filters were placed on top of a cold stage within a chamber that is flushed with dry nitrogen gas to prevent water condensation that is cooled at a constant rate of $1\,^{\circ}\mathrm{C\,min^{-1}}$ until temperatures of $\sim -35\,^{\circ}\mathrm{C}$. Droplet freezing was recorded, and the resulting videos were manually analysed to determine the fraction of droplets frozen at each temperature and then the INP concentration. At least one handling blank experiment was performed for every flight.

Handling blank filters were prepared and transported in the same way as the measurement filters, including loading the filters into the sampling system on the aircraft and briefly opening (for a second or so) and closing the inlet valves that allow air to pass through the filters. Hence, the handling blank should provide information on sources of contamination throughout the handling of the filter. A disadvantage of the droplet-on-filter technique is that each sample can only be analysed once, which makes it incompatible with standard heat tests such as the ones described by Daily et al. (2022). However, the great advantage of the droplet-on-filter technique over techniques where particles are washed off a filter into a volume of water is that it is around 20 times more sensitive than a typical wash-off assay employing 1 µL droplets (depending on the details of the freezing assays). This enhanced sensitivity is very important given that aerosol sampling durations are typically only a few tens of minutes long.

The frozen droplet fraction (the fraction of droplet that were frozen as a function of temperature) produced by our samples, along with those produced by the handling blank filters, is shown in Fig. 2a. While the frozen fraction for

https://doi.org/10.5194/acp-23-13819-2023

Table 1. Details of the samples collected during the MACSSIMIZE campaign. PTFE position refers to which inlet was used to collect the PTFE sample in each run. The other line was used to collect the polycarbonate sample. In order to determine if the sample was collected within the boundary layer (BL) or in the free troposphere (FT), we looked at the temperature and potential temperature profiles. Stored filters were kept for a few hours or days at −18 °C, while the rest of them were analysed immediately after collection without any long-term storage. The given altitude values correspond to the average of each run. The mean values of the air temperature across the run were derived from the Rosemount deiced temperature sensor, while the dew temperature is given by the Buck CR2 Hygrometer of the BAe-146. Dew temperature could not be calculated for all runs due to technical problems. The aerosol number concentration corresponds to the range of ∼0.1 to ∼3 µm and it has been calculated using the PCASP instrument. Blank entries correspond to a filter that was not collected or the instruments not working.

Sample	Date (2018)	Start time (UTC)	End time (UTC)	GPS altitude (m)	Radar altitude (m)	BL or FT	Vol. PC (L)	Vol. tef. (L)	PTFE position	Stored	Temperature (°C)	Dew temperature (°C)	Aerosol concentration (cm^{-3})
C085_1	03/11	22:22	22:34	475	474	FT	466	312	Up	No	−11.1	−14.4	–
C085_3	03/11	23:18	23:40	604	546	FT	461	355	Low	No	−5.4	−10.6	–
C086_1	03/13	21:14	21:22	38	38	BL	212	159	Low	No	−16.8	–	76.4
C086_2	03/13	21:29	21:49	138	139	BL	231	143	Up	No	−17.9	−18.3	75.9
C086_3	03/13	22:11	22:31	386	387	Intersection	644	209	Low	No	−11.3	−14.1	35.3
C087_1	03/16	20:44	21:26	310	309	BL	1047	565	Low	No	−19.7	–	68.9
C087_2	03/16	21:33	22:03	304	305	BL	965	447	Up	No	−16.4	–	61.2
C087_3	03/16	22:30	22:44	536	491	FT	392	217	Low	Yes	−13.6	–	46.8
C089_1	03/18	18:01	18:42	584	522	FT*	1198	714	Low	No	−21.3	−20.2	40.3
C089_2	03/18	18:49	19:17	573	506	FT*	–	398	Low	No	−21.2	−19.3	45.2
C089_3	03/18	19:28	19:48	591	557	FT*	404	214	Up	Yes	−20.9	−18.8	47.7
C090_1	03/20	20:15	20:38	547	487	FT*	735	349	Low	No	−15	−15.4	62.1
C090_2	03/20	20:53	21:26	563	503	FT*	488	409	Up	No	−14.6	−15.6	62.3
C091_2	03/21	18:27	18:56	122	123	FT*	1187	376	Up	No	−28	–	63.6
C091_3	03/21	19:01	19:14	295	297	FT*	644	203	Low	Yes	−25.7	–	63.9
C091_4	03/21	19:21	19:51	71	68	FT*	635	635	Up	No	−29.8	−27.4	31.8

* For all the runs in the C089, C090, and C091, the flight did not descend low enough to determine the exact depth of the BL. Hence, it was assumed that the runs occurred above the BL.

the sample filters was generally shifted to warmer temperatures than the handling blanks, many of the samples overlapped with the range defined by the handling blanks. Hence, it was necessary to account for influence of the background from the measurements. The background subtraction procedure and the INP concentration calculations are detailed in Appendix A. Briefly, we converted our cumulative fraction frozen values for the samples and handling blanks into the differential INP spectrum, $k(T)$, in units of INP per unit temperature (Vali, 1971, 2019); k is the number of INPs that become active in a temperature interval. This allowed us to define a limit of detection and then apply a criterion to separate samples that show a significant signal above this from the ones that do not. Data points whose error bars did not overlap with the error bars associated with the handling blank were considered to be above the limit of detection. The error bars of the differential concentrations of the samples represent a confidence level of 68 %, while the error bars of the background represent the standard deviation of all the measured handling blanks. Background subtraction was applied to data points above the limit of detection (k_{sample}–$k_{\text{background}}$) using a similar approach to Vali (2019). The cumulative INP spectrum, the common way of presenting INP data, was then derived using the background-corrected values of k.

A subset of the polycarbonate filters was analysed using scanning electron microscopy with energy dispersive spectroscopy (SEM-EDS) to study aerosol size-resolved composition. The analysis was carried out in the Leeds Electron Microscopy And Spectroscopy centre (LEMAS) at the University of Leeds. Filters were transported to the University of Leeds and then stored at ~ -18 °C until analysis. This technique can be used to obtain the morphological and chemical properties of individual aerosol particles within the sample. The subset of samples was coated with a 30 nm layer of iridium, and the SEM-EDS analysis was performed using an accelerating voltage of 20 KeV. The scanning and acquisition of EDS spectrums is done using a semi-automatic method with the Aztec Feature Software by Oxford Instruments. Our method captures the morphology and chemical signature of particles down to 0.2 or 0.3 µm depending on the sample. Particles are detected based on their contrast in the secondary electron images, although some artefacts were removed manually. Each particle is then classified into a defined composition category based on its chemical composition. The morphological and composition category of each particles is used to obtain statistics about the size-resolved composition of the aerosol samples. A more detailed description of the technique can be found in Sanchez-Marroquin et al. (2019).

In parallel with the filter sampling, we make use of FAAM's underwing optical particle counters. One of these counters is the Passive Cavity Aerosol Spectrometer Probe 100-X (PCASP), manufactured by Particle Measurement Systems, which measures aerosol particles in the 0.1 to ~ 3 µm range. The second counter is the Cloud Droplet Probe (CDP) by Droplet Measurement Technologies that measures aerosol particles and droplets with sizes from ~ 3 to 50 µm. A detailed description of these instruments and their calibration can be found in Rosenberg et al. (2012).

The Hybrid Single-Particle Lagrangian Integrated Trajectory (HYSPLIT) model was used to calculate 5 d back trajectories of sampled air masses (Stein et al., 2015; Rolph et al., 2017) and is shown in Sect S1. The back trajectories show that in many cases air masses remained near or over Alaska and northern Canada before sampling. However, the back trajectories corresponding to the C085 flight arrived mostly from the southwest. Most of the trajectories suggest that the air mostly stayed at altitudes below 1000 m above sea level in the 5 d prior to sampling. At the time of sampling, most of the sea and land surfaces were covered by sea ice or snow (Fig. 1), which most likely suppressed any local aerosol sources. However, local sources of marine aerosol particles may still occur due to open leads (May et al., 2016; Kirpes et al., 2019; Chen et al., 2022).

3 INP concentrations in the western North American Arctic

The background-corrected cumulative INP concentrations are shown in Fig. 2b. Hollow markers indicate measurements consistent with the limit of detection, where the lower error bar goes to zero, while filled markers correspond to a cumulative INP concentration above the limit of detection. Using a 68 % confidence interval, approximately 70 % of the differential spectra binned data were not significantly above the limit of detection, and around half of the data points in the cumulative INP spectra shown in Fig. 2b show INP concentrations consistent with zero (i.e. not above the detection limit). The reported INP concentrations are always below 0.1 and 1 L^{-1} at -15 and -20 °C, respectively. However, given the fact that a substantial percentage of the data are not above the detection limit, the real values of some of these samples may be well below these values. A more detailed daily representation of the INP concentrations is shown in Fig. A3.

INP concentrations across the Arctic vary significantly depending on the time of the year and location (Creamean et al., 2018; Si et al., 2019; Wex et al., 2019). Hence, in order to compare to the pertinent data, we show our INP concentrations alongside literature data collected for a similar location and time of the year in Fig. 3a (we restricted the literature datasets from February to April). Some of our reported INP concentrations are above some of the values measured using a droplet freezing assay on filters collected the surface by Creamean et al. (2018) and Wex et al. (2019) and filters collected on an aircraft and processed using a dynamic developing chamber at water saturation by Borys (1989). Creamean et al. (2018) reported INP concentrations at -25 °C up to 0.1 L^{-1} on the north coast of Alaska in March. Measurements performed by Wex et al. (2019) in a close location

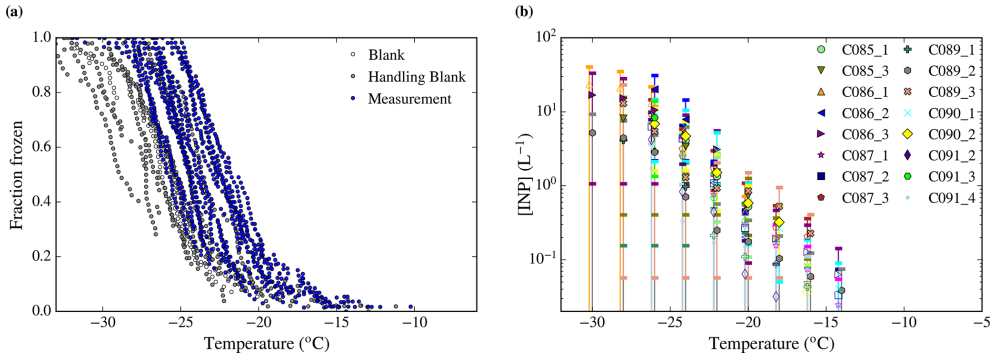

Figure 2. **(a)** Fraction of droplets frozen for all filter samples, as well as blanks and handling blanks. **(b)** INP particle concentrations for each filter sample. Data points corresponding to the upper limits (open symbols) have been shifted 0.2 °C along the x axis for clarity. The way in which the INP concentrations, upper limits, and uncertainties have been calculated is shown in Appendix A. The criteria to determine if a measurement is above the limit of detection is based on 68 % confidence intervals.

(Utqiaġvik) indicate that INP concentrations ranging from $\sim 10^{-4}$ to $10^{-2}\,\mathrm{L}^{-1}$ at −10 °C in March. The more active samples reported by Wex et al. (2019) form a consistent INP spectrum with our more active samples, but unfortunately there is no direct overlap. Borys (1989) reported INP concentrations of 0.001 to $0.3\,\mathrm{L}^{-1}$ at −25 °C measured from an aircraft at a similar location and time of the year. These values are of course consistent with our samples where we report upper limits, but some of our samples clearly had substantially higher INP concentrations than the range reported by Borys (1989). Hiranuma et al. (2013) also report INP measurements using an airborne continuous-flow diffusion chamber (CFDC) during the Indirect and Semi-Direct Aerosol Campaign (ISDAC) in a very similar study region to ours but in April rather than March. We have only compared our measurements with theirs at water saturation, which happened to be during a relatively high INP period. This INP value of $5.6 \pm 3.5\,\mathrm{L}^{-1}$ at −22 °C is consistent with our highest recorded INP concentrations. Overall, this comparison with measurements in previous years at a similar location and time of year indicates that the INP concentrations are rather variable, ranging over at least 3 orders of magnitude at −20 °C.

Our measurements have also been presented alongside a compilation of INP measurements from across the Arctic carried out throughout the year (Fig. 3b). Our dataset is well within the range of literature INP measurements from across the Arctic. Around 50 % of our data points were below detection limit (and not shown in Fig. 3); hence, we are only able to report INP concentrations when their values are relatively high. The picture that emerges in the Arctic is a region of highly variable INP concentrations, where INP concentrations vary spatially as well as temporally (seasonally as well as on shorter timescales). This variability is likely related to a combination of transport from local and remote sources of INP and sinks both locally and along those transport routes. This high variability in INP concentrations will affect primary ice production in clouds, with more INP leading to greater ice concentrations that may or may not be amplified by secondary production processes. Intriguingly, several authors report that greater INP concentrations leads to more ice in Arctic cloud and vice versa (Rogers et al., 2001; Hiranuma et al., 2013).

A handful of Arctic measurements of INP have been made from aircraft (Hartmann et al., 2020; Sanchez-Marroquin et al., 2020; Prenni et al., 2009; Hiranuma et al., 2013), and it is these measurements that produce many of the highest observed Arctic INP concentrations, rather than those made on the ground. However, aircraft sampling is often limited by the volume of air that can be sampled due to restrictions in flight lengths and other technical limitations. This necessarily biases the results to relatively high INP concentrations. For example, Rogers et al. (2001) report that 50 % of the 10 s averaged data was zero (i.e. below detection limit). Given that the Arctic atmosphere is highly stratified, it would be interesting to perform simultaneous measurements at the surface and from an aircraft to explore how or if INP at the surface are related to those higher in the boundary later and those in the free troposphere.

4 SEM-EDS size-resolved composition analysis

The equivalent circular diameter size distributions obtained with the SEM-EDS technique were compared with the average size distributions for the same sampling periods measured using the underwing optical particle counters on-board of the FAAM BAe-146. The analysis is shown in Fig. 4 alongside the size-resolved chemical composition of the analysed samples. The number size distribution is multiplied by the fraction of particles in each category and binned to calculate the number size distribution of each category. These number size distributions are then turned into surface area size distributions and integrated to obtain the surface area of each category, as shown in Table 2.

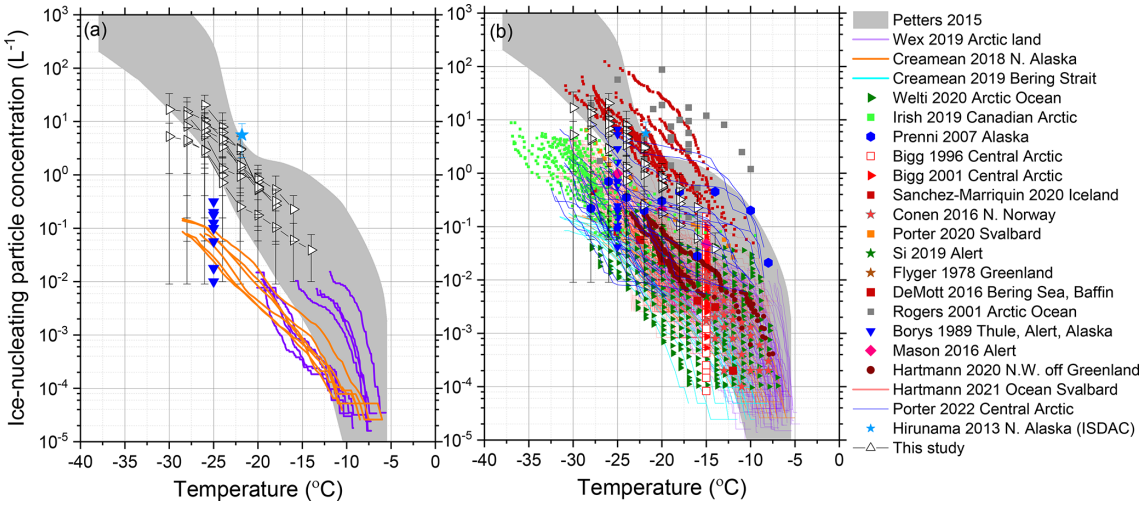

Figure 3. INP concentrations from the present study compared with literature data. We only show our data that were above the background (limiting values are included in Fig. 2). Note that these data are above the limit of detection based on 68 % confidence intervals. The left panel is limited to a comparison with previous measurements at nearby locations at a similar time of year (February, March and April) (Borys, 1989; Creamean et al., 2018; Wex et al., 2019; Hiranuma et al., 2013). We also limit this comparison to data recorded at or above water saturation, which limits the data from Hiranuma et al. (2013) to a single point during what they describe as a relatively high-INP-concentration event. Note that for the dataset of Wex et al. (2019), the concentrations increased through this period, with the two highest INP spectra being from April. The right panel is a comparison with Arctic data in general from any time of the year and any location (Flyger and Heidam, 1978; Borys, 1989; Bigg, 1996; Rogers et al., 2001; Bigg and Leck, 2001; Prenni et al., 2007; Hiranuma et al., 2013; Conen et al., 2016; DeMott et al., 2016; Mason et al., 2016; Creamean et al., 2018, 2019; Wex et al., 2019; Irish et al., 2019; Si et al., 2019; Porter et al., 2020, 2022; Sanchez-Marroquin et al., 2020; Welti et al., 2020; Hartmann et al., 2020, 2021). The mid-latitude data range given by Petters and Wright (2015) is also shown.

Table 2. Surface area of dust and sea spray aerosol from SEM-EDS analysis. The dust limit of detection corresponds to the upper limit of the dust concentration detected on the handling blank filter based on 1 standard deviation. Note that the given dust and sea spray aerosol percentages refer to surface area percentages. The limit of detection of sea spray aerosol particles has not been indicated because the presence of this type of particle in the handling blank is negligible. Further information on the size-resolved composition of the handling blanks and a discussion about it can be found in Sanchez-Marroquin et al. (2019).

Sample	Dust area ($\mu m^2\ cm^{-3}$)	Dust limit of detection ($\mu m^2\ cm^{-3}$)	Dust area percentage	Sea spray aerosol area ($\mu m^2\ cm^{-3}$)	Sea spray area percentage
C087_1	0.75	0.042	13.9	3.97	73.4
C089_3	0.57	0.15	38.1	0.26	17.1
C090_1	1.21	0.083	65.5	0.16	8.9
C091_2	0.53	0.051	11.3	2.79	59.5

The analysed samples exhibited low aerosol concentrations relative to other locations where we have used this technique, especially for the coarse mode. In this study, almost no particles above 10 µm were detected, in contrast to samples from around Iceland, the eastern tropical Atlantic, and the southeast of the United Kingdom analysed using the same or similar techniques, where significant amounts of aerosols in between 10 and 20 µm were detected (Price et al., 2018; Sanchez-Marroquin et al., 2019, 2020, 2021). Most of the detected particles were below ∼ 2 µm. At sizes below ∼ 3 µm, the comparisons between the optical probes and the SEM-EDS size distributions are consistent in most cases, with an undercounting at the lower end of the SEM-EDS technique (∼ 0.3 µm). This undercounting is related to the difficulty in observing small organic-rich particles and has been discussed in Sanchez-Marroquin et al. (2019). At sizes above ∼ 3 µm, the optical probes and SEM-EDS size distributions showed a comparable amount of detected particles in samples C089_3 and C090_1. However, for samples C087_1 and C091_2, the optical counters detected a larger concentration of particles with sizes ∼ 5 to 10 µm than the SEM analysis of the filters. Similar discrepancies have been observed previously with these instruments in another low-aerosol environment (Young et al., 2016) and were attributed to regions of high humidity even if the average humidity in a run should not have led to substantial hygroscopic growth.

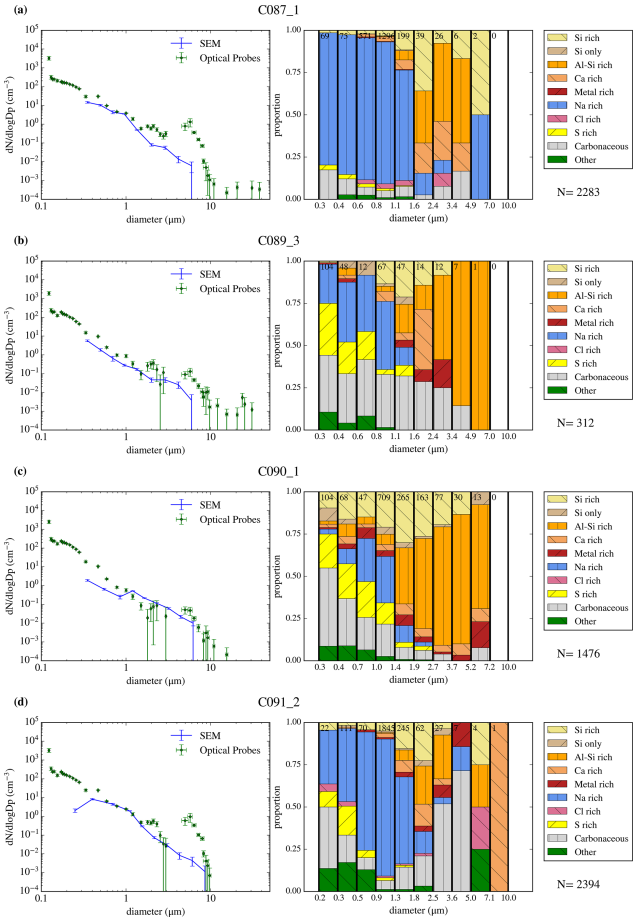

Figure 4. Results of SEM-EDS analysis of each analysed sample **(a–d)** showing a comparison between the SEM-EDS and PCASP-CDP number size distribution (left) and number-size-resolved composition fractions (right).

In dust plumes near Iceland and in aerosol around the UK where there was a significant coarse mode, the agreement between CDP and SEM tended to be good. We note CDP is designed for cloud droplets, and we are using it at the edge of its capability for larger aerosol particles; hence, there may be some biases that seem more significant in low-aerosol environments.

In terms of chemical composition, the samples were mainly dominated by sea spray (Na rich) and mineral dust (Si rich, Si only, Al and Si rich and Ca rich) particles. There were some smaller contributions of S-rich particles (likely sulfates) and carbonaceous particles (likely black carbon or organic material). This is consistent with other SEM-EDS studies of the aerosol samples collected in the Alaskan Arctic from the ground (Chen et al., 2022; Creamean et al., 2018; Kirpes et al., 2018; Gunsch et al., 2017) or during a ship campaign (Kirpes et al., 2020). However, we tend to observe larger fractions of dust aerosol particles, particularly in the sample C090_1, where this type of aerosol constituted ∼ 65 % of the surface area of the sample.

In this dataset, nearly all particles in the Na-rich category were dominated by the presence of Na and Cl, having traces of other elements (such as S on some occasions), consistent with sea spray particles. As a consequence, we will refer to particles in this category as sea spray aerosol particles. Some carbonaceous particles were also detected through most sizes, and there were significant contributions of S-rich aerosol, particularly in the accumulation mode. As shown in Fig. 4 and Table 2, the surface area of samples C087_1 and C091_2 was dominated by sea spray aerosol particles with sizes around ∼ 1 µm. In Sect. S1 in the Supplement, it is shown that most of the air masses associated with these samples had been circulating above the Arctic Ocean at relatively low altitude (below 1000 m) before sampling took place. This is consistent with the fact that sea spray aerosol particles are normally emitted by a bubble bursting at the surface of the oceans (Lewis and Schwartz, 2004). It is possible that the detected sea spray aerosol in our study was transported from ice-free oceans. However, Sect. S1 indicates that the closest ocean masses were almost fully covered by sea ice (with some open leads) during the campaign, and the majority of the sampled air masses did not pass by the open oceans prior to sampling. Hence, it is possible that the sea spray particles had been emitted from open leads in the sea ice, as this is thought to be a source of sea spray aerosol in the region (May et al., 2016; Kirpes et al., 2019; Chen et al., 2022). It is also possible that some of the sea spray aerosol has been directly emitted from the sea ice through blowing snow events (Yang et al., 2008; Huang and Jaeglé, 2017; Frey et al., 2020).

Particles in the Si-rich, Si-only, Al- and Si-rich, and Ca-rich categories have a chemical composition consistent with mineral dust particles, so we will refer to them collectively as mineral dust. However, it should be kept in mind that the composition of particles in these categories is also consistent with some types of combustion ash or volcanic ash. Mineral dust particles were present in all of the samples, particularly with sizes between 1 and 5 µm, constituting a substantial percentage of its surface area, as shown in Table 2. This was particularly the case in the sample C090_1, where 65 % of the surface area was given by mineral dust particles. Although we cannot fully determine the relative contribution of different sources to the detected mineral dust, several arguments suggest that the sampled mineral dust originated from the low-latitude deserts. The back trajectory analysis shown in Sect. S1 suggests that most of the air masses had been circulating around the sampling location prior to sampling for ∼ 5 d. However, the majority of the potential high-latitude dust sources were covered by snow at this time, so it seems unlikely that this mineral dust is related to natural emissions, although we cannot rule out sources associated with human activities along the coast (e.g. Purdue Bay oil fields). Mineral dust originating from the Sahara and central Asia is known to be transported to the Arctic, especially in late winter and

early spring when this study took place (VanCuren et al., 2012; Fan, 2013; Huang et al., 2015; Francis et al., 2018; Shi et al., 2022; Zhao et al., 2022). This is consistent with the back trajectories associated with the samples collected on the C085 flight, which originate from Asia. Almost all of the mineral dust particles found in this study had sizes below 5 µm, and it is known that dust particles have a lifetime of many days and thus can conceivably be transported to Alaska from distant sources (Huneeus et al., 2011; Ménégoz et al., 2012). Once in the Arctic, accumulation mode aerosol has a lifetime extending to months during winter and spring, when removal processes are weak (Carslaw, 2022). The small sizes of dust particles found in this campaign contrast with results obtained using similar techniques on samples collected closer to dust sources, where dust particles with sizes above 10 µm are frequent (Price et al., 2018; Ryder et al., 2018; Sanchez-Marroquin et al., 2020). Although this evidence suggests that most of our dust likely originated in arid lower-latitude deserts, high-latitude dust could still contribute to the dust budget or even dominate it during other times of the year such as autumn (Groot Zwaaftink et al., 2016; Shi et al., 2022).

As shown in Table 2, C087_1 and C091_2 samples have a larger surface area of sea spray aerosol particles (Na rich) than mineral dust, whereas sample C090_1 is dominated by the presence of mineral dust. Hence, it is reasonable to ask if the mineral dust or organic material associated with sea spray is the more important INP type in these samples. To estimate the relative contribution of mineral dust and sea spray aerosol to the INP population, we present the expected INP concentrations based on the SEM-EDS surface areas in Fig. 5, in comparison with the measured INP concentrations. The INP concentrations expected from the SEM-EDS analysis were calculated assuming a dust containing 10 % of K-feldspar (Harrison et al., 2019) (the ice-active component of desert dust) and the parameterization of fertile soils given by O'Sullivan et al. (2014). Note that the latter is very similar to the desert dust parameterization given by Ullrich et al. (2017). For the pristine sea spray INP, the parameterization given by McCluskey et al. (2018) that links INP concentration and aerosol surface area has been used. As shown, even in the cases where there is more sea spray aerosol than mineral dust (C087_1 and C091_2), the minimum contribution of mineral dust INP is orders of magnitude above the INPs produced by the pristine sea spray aerosol particles. It is possible that the sea spray in this location was more active than defined by McCluskey et al. (2018); however, the INP concentrations calculated based on the presence of dusts better explains the observed INP concentrations measured using the droplet freezing assay at the lower end of the temperature spectrum. At the higher end of the temperature spectrum, the measured INP concentrations are above those expected from a 10 % K-feldspar dust but are consistent with the fertile soil dust parameterization. It is known that fertile soil dusts contain biological ice-nucleating material (O'Sullivan et al., 2014), and hence this suggests that the samples from Alaska contained some biological ice-nucleating material (either from marine or terrestrial sources). Although our INP concentrations would also be comparable with those predicted using the desert dust parameterization by Ullrich et al. (2017), the latter is usually higher than the activity of samples of airborne desert dust at temperatures greater than about −20 °C from other studies (Boose et al., 2016; Price et al., 2018; Harrison et al., 2022; Reicher et al., 2018; Gong et al., 2020). It has been suggested that dust that has been transported far from its source regions is less active than arid soil dusts that have been recently aerosolized, and there also appears to be substantial differences in the activity of dust from different source regions (Boose et al., 2016; Harrison et al., 2022). Hence, we suggest that the enhanced ice nucleation ability of our samples is perhaps due to the presence of biological material. This is consistent with other studies that also provided evidence that Arctic INP samples have a substantial biological component (Wex et al., 2019; Creamean et al., 2019; Santl-Temkiv et al., 2019; Porter et al., 2022).

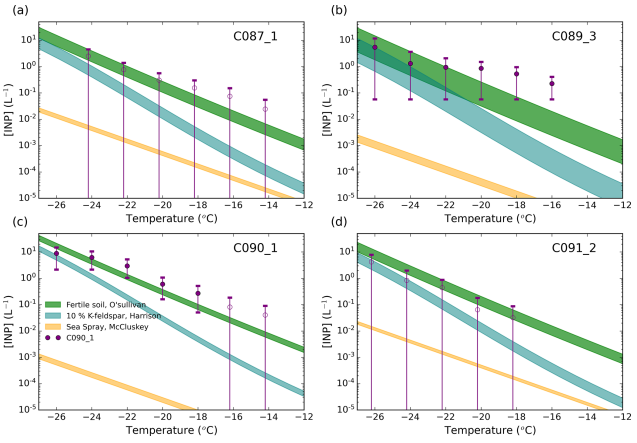

Figure 5. Predicted INP concentration of the SEM-EDS samples compared with the INP measurements at −20 °C. The dust INP prediction has been calculated by applying different ice nucleation parameterizations to the surface area of dust calculated from the SEM-EDS analysis. The O'Sullivan et al. (2014) data were used for fertile soils, and a dust containing 10 % K-feldspar (Harrison et al., 2019) has been used. The NaCl INP prediction has been obtained by applying the sea spray aerosol parameterization from McCluskey et al. (2018) to the SEM-EDS sea spray aerosol surface area. The purple points correspond to our INP measurements or upper limits based on 68 % confidence intervals (Appendix A).

5 Conclusions

In this study, we present a new dataset of INP and SEM-EDS aerosol size-resolved composition measurements in the western North American Arctic in March 2018. Back trajectory analysis suggests that most of these air masses spend the preceding 5 d circulating over or near Alaska and north-

ern Canada where local sources of primary aerosol were suppressed by snow and ice cover. Observed INP concentrations were at or close to the limit of detection of the measuring technique, being always below 0.1 and $1\,L^{-1}$ at -15 and $-20\,°C$, respectively. SEM-EDS analysis revealed that samples are mostly dominated by the presence of mineral dust and sea spray aerosol particles, with some contributions of sulfur-rich and carbonaceous particles. The mineral dust is most likely sourced from the low-latitudes, rather than local high-latitude dust sources. Our analysis shows that mineral dust contributes more to the INP population than sea spray, despite sea spray being more abundant in some samples. However, it appears that the ice-active mineral K-feldspar cannot account for all of the observed INPs, especially above $\sim -22\,°C$. This suggests that there is another INP type that controls the INP spectrum above $-22\,°C$; these particles may be biogenic in origin, but where this biogenic ice-nucleating material might be derived from is unclear. More work is clearly required to understand the sources and nature of INP in the winter and early springtime Arctic.

Appendix A: Upper-limit determination and background subtraction of the ice nucleation experiments

As shown in Fig. 2a, most of the fraction of frozen droplets produced by the collected samples were comparable or only slightly above to the ones produced by the handling blanks. Hence, we established criteria to separate data points of the INP spectrum that are not significantly above the limit of detection of the instrument. The analysis is performed using the differential spectrum of the ice nucleus rather than the cumulative spectrum, which is normally used to display and compare ice nucleation data such as INP concentrations and densities of active sites (Vali, 1971, 2019). First, we create a histogram with the number of freezing events per temperature interval per sample. This is done for all the samples and handling blanks, with temperature intervals of 2 °C. We transform the number of freezing events per interval of each sample into the differential INP spectrum, $k(T)$, using Eq. (A1) (Vali, 2019).

$$k(T) = -\frac{1}{V_d \Delta T} \ln\left(1 - \frac{\Delta N}{N(T)}\right) \quad \text{(A1)}$$

In Eq. (A1), V_d is the droplet volume, ΔT is the temperature interval, $\Delta N$is the number of frozen droplets between T and (T-ΔT), and $N(T)$ is the number of unfrozen droplets at T. The $k(T)$ values of the handling blanks is shown in Fig. A1, alongside the mean value of each interval and its standard deviation. Note that many of the temperature intervals had zero freezing events, corresponding to k equal to zero. These zero values cannot be seen in Fig. A1, but they have been included in the means and standard deviations. The mean and standard deviation of the k values produced by each handling blank has been compared with the k values corresponding to each sample. The uncertainty in the k values associated with each sample has been calculated using a very similar Monte Carlo simulation as used previously (Vali, 2019) using a 68 % interval. The k values associated with each sample were individually compared with the mean and standard deviation of the k values of the handling blanks. A data point was considered above the limit of detection when its lower error yields above the mean plus standard deviation of the blanks. Background subtraction was applied to data points significantly above the limit of detection. This was done by subtracting the mean of the k values of the handling blanks. The error of the background-subtracted point was calculated by square rooting the quadratic sum of the error of the k_{sample} and $k_{background}$. Two examples of the comparisons between samples and the handling blanks are shown in Fig. A2. Figure A2a corresponds to a case where no data point was higher than the limit of detection, while Fig. A2b corresponds to a case where most of the data points were significantly above the limit of detection. Note that all of the data measured on 16 March (flight C087) have been flagged as an upper limit. This is because the handling blank experiment carried out on that day was unusually high, being compatible with all of the measurements.

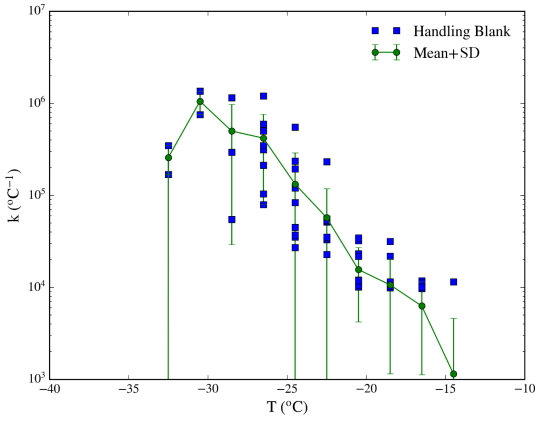

Figure A1. Differential spectrum of the ice nucleus of all the handling blanks performed during this campaign. Data are shown in blue, while the mean and standard deviation of the data of each bin are shown in green.

The background-corrected $k(T)$ was integrated into the cumulative spectrum of active sites, $K(T)$, using Eq. (A2) (Vali, 1971, 2019).

$$K(T) = \sum_{T=0}^{T} k(T)\,\Delta T \quad \text{(A2)}$$

INP concentrations were calculated from $K(T)$ using Eq. (A3), where V_d is the droplet volume, A_{fil} is the area of the filter, V_a is the sampled air volume, and α is the contact surface of the droplets. For this study, we used the same

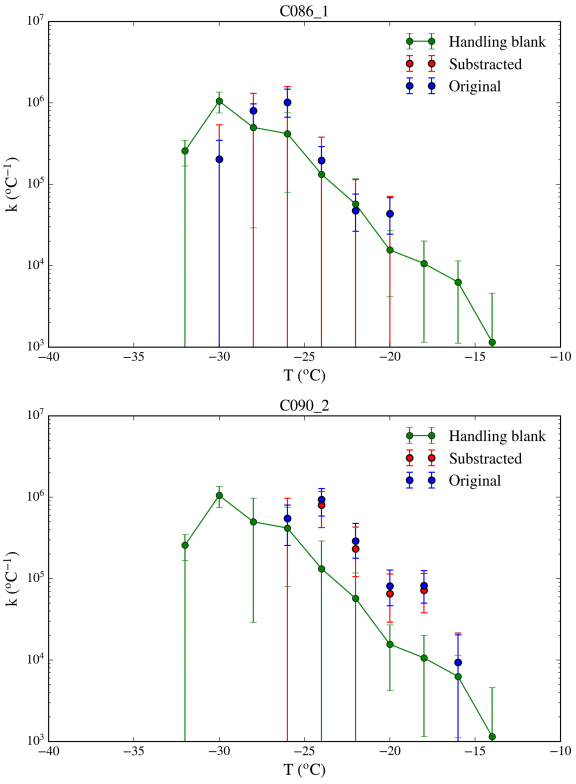

Figure A2. Examples of a comparison between the handling blank mean with two samples. None of the data points of sample C086_1 are significantly above the background. However, most of the data points associated with sample C090_2 are more than one error bar above the data produced by the handling blanks, and they have been background subtracted.

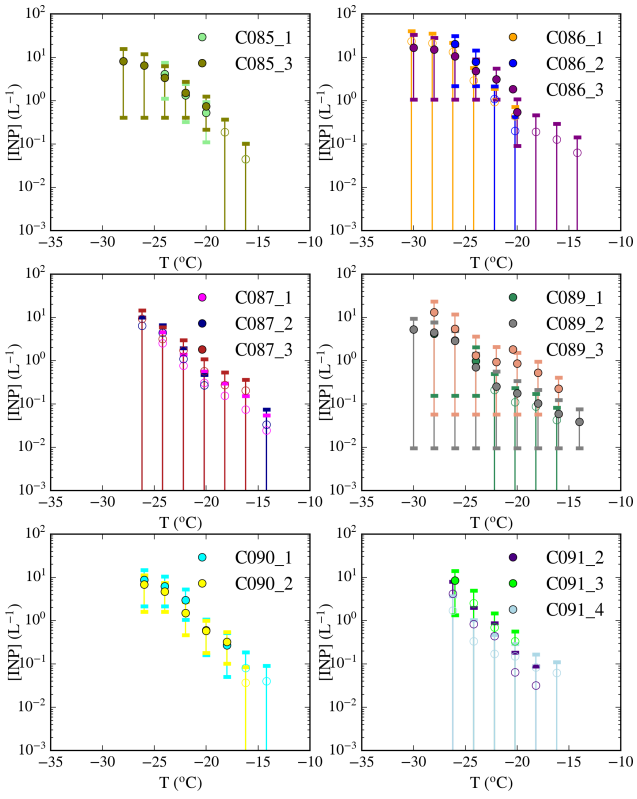

Figure A3. INP concentrations and upper limits shown in Fig. 2 separated by sampling day. A list of the days when these samples were collected is shown in Table 1. Note that full markers correspond to measurements above the limit of detection, while hollow markers correspond to upper limits. This has not been specified in the legend as some samples have both upper limits and measurements at the same time.

values as Sanchez-Marroquin et al. (2021).

$$\mathrm{INP}(T) = \frac{K(T)\, V_\mathrm{d} A_\mathrm{fil}}{V_\mathrm{a} \alpha} \tag{A3}$$

A k value that was not significantly above the limit of detection has been represented with lower bars going to zero in the INP spectrum (meaning upper limit of the INP concentration). However, if a k value not significantly above the limit of detection was preceded by a value that was above the limit of detection, then as a result of the cumulative nature of the reported INP concentration the corresponding value is reported with a filled symbol, but the lower bound of the error bar does not change since it is possible that no new INP were present in that temperature interval. In Fig. A3 one can see the INP concentrations of all of the samples collected in this study for each day.

Data availability. All data needed to evaluate the conclusions in the paper are present in the paper and/or the Supplement. The digitalized data are available from https://doi.org/10.5518/1401 (Sanchez-Marroquin and Murray), with each of the flights can be found at https://catalogue.ceda.ac.uk/uuid/b04281cc10c44d9dab1eb2e4eb19d5b8 (Facility for Airborne Atmospheric Measurements; Natural Environment Research Council; Met Office; and similar for the other samples).

Supplement. The supplement related to this article is available online at: https://doi.org/10.5194/acp-23-13819-2023-supplement.

Author contributions. Aerosol measurements during the MACSSIMIZE campaign were organized by ASM, JBM, and BJM. ASM and BJM worked on the manuscript with contributions from all authors. The field work was carried out by ASM and JBM. ASM performed all of the experimental measurements (INP analysis and SEM-EDS). The SEM-EDS technique was developed by ASM and ITB. The back trajectory analysis was carried out by SLB and ASM. All of the authors contributed to the discussion.

Competing interests. The contact author has declared that none of the authors has any competing interests.

Disclaimer. Publisher's note: Copernicus Publications remains neutral with regard to jurisdictional claims in published maps and institutional affiliations.

Acknowledgements. We are grateful to all the people involved in the MACSSIMIZE campaign led by Chawn Harlow (UK Met Office). The samples were collected using the FAAM BAe-146-301 Atmospheric Research Aircraft, flown by Airtask Ltd., maintained by Avalon Aero Ltd., and managed by FAAM Airborne Laboratory, which is jointly operated by UKRI and the University of Leeds. We acknowledge the Centre for Environmental Data Analysis for the access to the FAAM datasets used here. We would also like to thank Duncan Hedges and Richard Walshlaw at the Leeds Electron Microscopy and Spectroscopy Centre.

Financial support. This research has been supported by the European Research Council, H2020 European Research Council (MarineIce, grant no. 648661), and the Natural Environment Research Council (grant nos. NE/R006687/1 and NE/T00648X/1).

Review statement. This paper was edited by Luis A. Ladino and reviewed by three anonymous referees.

References

Bigg, E. K.: Ice forming nuclei in the high Arctic, Tellus B, 48, 223–233, https://doi.org/10.1034/j.1600-0889.1996.t01-1-00007.x, 1996.

Bigg, E. K. and Leck, C.: Cloud-active particles over the central Arctic Ocean, J. Geophys. Res.-Atmos., 106, 32155–32166, https://doi.org/10.1029/1999jd901152, 2001.

Boose, Y., Sierau, B., García, M. I., Rodríguez, S., Alastuey, A., Linke, C., Schnaiter, M., Kupiszewski, P., Kanji, Z. A., and Lohmann, U.: Ice nucleating particles in the Saharan Air Layer, Atmos. Chem. Phys., 16, 9067–9087, https://doi.org/10.5194/acp-16-9067-2016, 2016.

Borys, R. D.: Studies of ice nucleation by Arctic aerosol on AGASP-II, J. Atmos. Chem., 9, 169–185, https://doi.org/10.1007/bf00052831, 1989.

Boucher, O., Randall, D., Artaxo, P., Bretherton, C., Feingold, G., Forster, P., Kerminen, V.-M., Kondo, Y., Liao, H., Lohmann, U., Rasch, P., Satheesh, S. K., Sherwood, S., Stevens, B., and Zhang, X. Y.: Clouds and Aerosols. In: Climate Change 2013: The Physical Science Basis, Contribution of Working Group I to the Fifth Assessment Report of the Intergovernmental Panel on Climate Change, edited by: Stocker, T. F., Qin, D., Plattner, G.-K., Tignor, M., Allen, S. K., Boschung, J., Nauels, A., Xia, Y., Bex, V. and Midgley, P. M., Cambridge University Press, Cambridge, United Kingdom and New York, NY, USA, https://www.ipcc.ch/site/assets/uploads/2018/02/WG1AR5_Chapter07_FINAL-1.pdf (last access: 25 April 2018), 2013.

Bullard, J. E., Baddock, M., Bradwell, T., Crusius, J., Darlington, E., Gaiero, D., Gassó, S., Gisladottir, G., Hodgkins, R., McCulloch, R., McKenna-Neuman, C., Mockford, T., Stewart, H., and Thorsteinsson, T.: High-latitude dust in the Earth system, Rev. Geophys., 54, 447–485, https://doi.org/10.1002/2016rg000518, 2016.

Carslaw, K. S.: Chapter 5 – Aerosol processes, in: Aerosols and Climate, edited by: Carslaw, K. S., Elsevier, 135–185, https://doi.org/10.1016/B978-0-12-819766-0.00007-9, 2022.

Ceppi, P., Brient, F., Zelinka, M. D., and Hartmann, D. L.: Cloud feedback mechanisms and their representation in global climate models, Wiley Interdisciplinary Reviews: Climate Change, 8, e465, https://doi.org/10.1002/wcc.465, 2017.

Chen, Q., Mirrielees, J. A., Thanekar, S., Loeb, N. A., Kirpes, R. M., Upchurch, L. M., Barget, A. J., Lata, N. N., Raso, A. R. W., McNamara, S. M., China, S., Quinn, P. K., Ault, A. P., Kennedy, A., Shepson, P. B., Fuentes, J. D., and Pratt, K. A.: Atmospheric particle abundance and sea salt aerosol observations in the springtime Arctic: a focus on blowing snow and leads, Atmos. Chem. Phys., 22, 15263–15285, https://doi.org/10.5194/acp-22-15263-2022, 2022.

Conen, F., Stopelli, E., and Zimmermann, L.: Clues that decaying leaves enrich Arctic air with ice nucleating particles, Atmos. Environ., 129, 91–94, https://doi.org/10.1016/j.atmosenv.2016.01.027, 2016.

Creamean, J. M., Kirpes, R. M., Pratt, K. A., Spada, N. J., Maahn, M., de Boer, G., Schnell, R. C., and China, S.: Marine and terrestrial influences on ice nucleating particles during continuous springtime measurements in an Arctic oilfield location, Atmos.

Chem. Phys., 18, 18023–18042, https://doi.org/10.5194/acp-18-18023-2018, 2018.

Creamean, J. M., Cross, J. N., Pickart, R., McRaven, L., Lin, P., Pacini, A., Hanlon, R., Schmale, D. G., Ceniceros, J., Aydell, T., Colombi, N., Bolger, E., and DeMott, P. J.: Ice Nucleating Particles Carried From Below a Phytoplankton Bloom to the Arctic Atmosphere, Geophys. Res. Lett., 46, 8572–8581, https://doi.org/10.1029/2019gl083039, 2019.

Creamean, J. M., Hill, T. C. J., DeMott, P. J., Uetake, J., Kreidenweis, S., and Douglas, T. A.: Thawing permafrost: an overlooked source of seeds for Arctic cloud formation, Environ. Res. Lett., 15, 084022, https://doi.org/10.1088/1748-9326/ab87d3, 2020.

Creamean, J. M., Barry, K., Hill, T. C. J., Hume, C., DeMott, P. J., Shupe, M. D., Dahlke, S., Willmes, S., Schmale, J., Beck, I., Hoppe, C. J. M., Fong, A., Chamberlain, E., Bowman, J., Scharien, R., and Persson, O.: Annual cycle observations of aerosols capable of ice formation in central Arctic clouds, Nat. Commun., 13, 3537, https://doi.org/10.1038/s41467-022-31182-x, 2022.

Daily, M. I., Tarn, M. D., Whale, T. F., and Murray, B. J.: An evaluation of the heat test for the ice-nucleating ability of minerals and biological material, Atmos. Meas. Tech., 15, 2635–2665, https://doi.org/10.5194/amt-15-2635-2022, 2022.

DeMott, P. J., Hill, T. C., McCluskey, C. S., Prather, K. A., Collins, D. B., Sullivan, R. C., Ruppel, M. J., Mason, R. H., Irish, V. E., Lee, T., Hwang, C. Y., Rhee, T. S., Snider, J. R., McMeeking, G. R., Dhaniyala, S., Lewis, E. R., Wentzell, J. J., Abbatt, J., Lee, C., Sultana, C. M., Ault, A. P., Axson, J. L., Diaz Martinez, M., Venero, I., Santos-Figueroa, G., Stokes, M. D., Deane, G. B., Mayol-Bracero, O. L., Grassian, V. H., Bertram, T. H., Bertram, A. K., Moffett, B. F., and Franc, G. D.: Sea spray aerosol as a unique source of ice nucleating particles, P. Natl. Acad. Sci. USA, 113, 5797–5803, https://doi.org/10.1073/pnas.1514034112, 2016.

Facility for Airborne Atmospheric Measurements; Natural Environment Research Council; Met Office: MACSSIMIZE: in-situ airborne observations by the FAAM BAE-146 aircraft. Centre for Environmental Data Analysis, date of citation, http://catalogue.ceda.ac.uk/uuid/cdecaea11e59472b8800d5d938a3c8ee (last access date: 19 June 2018), 2018.

Fan, S.-M.: Modeling of observed mineral dust aerosols in the arctic and the impact on winter season low-level clouds, J. Geophys. Res.-Atmos., 118, 11161–111174, https://doi.org/10.1002/jgrd.50842, 2013.

Flyger, H. and Heidam, N. Z.: Ground level measurements of the summer tropospheric aerosol in Northern Greenland, J. Aerosol Sci., 9, 157–168, https://doi.org/10.1016/0021-8502(78)90075-7, 1978.

Francis, D., Eayrs, C., Chaboureau, J. P., Mote, T., and Holland, D. M.: Polar Jet Associated Circulation Triggered a Saharan Cyclone and Derived the Poleward Transport of the African Dust Generated by the Cyclone, J. Geophys. Res.-Atmos., 123, 11899–811917, https://doi.org/10.1029/2018jd029095, 2018.

Frey, M. M., Norris, S. J., Brooks, I. M., Anderson, P. S., Nishimura, K., Yang, X., Jones, A. E., Nerentorp Mastromonaco, M. G., Jones, D. H., and Wolff, E. W.: First direct observation of sea salt aerosol production from blowing snow above sea ice, Atmos. Chem. Phys., 20, 2549–2578, https://doi.org/10.5194/acp-20-2549-2020, 2020.

Gong, X., Wex, H., van Pinxteren, M., Triesch, N., Fomba, K. W., Lubitz, J., Stolle, C., Robinson, T.-B., Müller, T., Herrmann, H., and Stratmann, F.: Characterization of aerosol particles at Cabo Verde close to sea level and at the cloud level – Part 2: Ice-nucleating particles in air, cloud and seawater, Atmos. Chem. Phys., 20, 1451–1468, https://doi.org/10.5194/acp-20-1451-2020, 2020.

Groot Zwaaftink, C. D., Grythe, H., Skov, H., and Stohl, A.: Substantial contribution of northern high-latitude sources to mineral dust in the Arctic, J. Geophys. Res.-Atmos., 121, 13678–613697, https://doi.org/10.1002/2016jd025482, 2016.

Gunsch, M. J., Kirpes, R. M., Kolesar, K. R., Barrett, T. E., China, S., Sheesley, R. J., Laskin, A., Wiedensohler, A., Tuch, T., and Pratt, K. A.: Contributions of transported Prudhoe Bay oil field emissions to the aerosol population in Utqiaġvik, Alaska, Atmos. Chem. Phys., 17, 10879–10892, https://doi.org/10.5194/acp-17-10879-2017, 2017.

Harrison, A. D., Lever, K., Sanchez-Marroquin, A., Holden, M. A., Whale, T. F., Tarn, M. D., McQuaid, J. B., and Murray, B. J.: The ice-nucleating ability of quartz immersed in water and its atmospheric importance compared to K-feldspar, Atmos. Chem. Phys., 19, 11343–11361, https://doi.org/10.5194/acp-19-11343-2019, 2019.

Harrison, A. D., O'Sullivan, D., Adams, M. P., Porter, G. C. E., Blades, E., Brathwaite, C., Chewitt-Lucas, R., Gaston, C., Hawker, R., Krüger, O. O., Neve, L., Pöhlker, M. L., Pöhlker, C., Pöschl, U., Sanchez-Marroquin, A., Sealy, A., Sealy, P., Tarn, M. D., Whitehall, S., McQuaid, J. B., Carslaw, K. S., Prospero, J. M., and Murray, B. J.: The ice-nucleating activity of African mineral dust in the Caribbean boundary layer, Atmos. Chem. Phys., 22, 9663–9680, https://doi.org/10.5194/acp-22-9663-2022, 2022.

Hartmann, M., Adachi, K., Eppers, O., Haas, C., Herber, A., Holzinger, R., Hünerbein, A., Jäkel, E., Jentzsch, C., Pinxteren, M., Wex, H., Willmes, S., and Stratmann, F.: Wintertime Airborne Measurements of Ice Nucleating Particles in the High Arctic: A Hint to a Marine, Biogenic Source for Ice Nucleating Particles, Geophys. Res. Lett., 47, e2020GL087770, https://doi.org/10.1029/2020gl087770, 2020.

Hartmann, M., Gong, X., Kecorius, S., van Pinxteren, M., Vogl, T., Welti, A., Wex, H., Zeppenfeld, S., Herrmann, H., Wiedensohler, A., and Stratmann, F.: Terrestrial or marine – indications towards the origin of ice-nucleating particles during melt season in the European Arctic up to 83.7° N, Atmos. Chem. Phys., 21, 11613–11636, https://doi.org/10.5194/acp-21-11613-2021, 2021.

Hawker, R. E., Miltenberger, A. K., Wilkinson, J. M., Hill, A. A., Shipway, B. J., Cui, Z., Cotton, R. J., Carslaw, K. S., Field, P. R., and Murray, B. J.: The temperature dependence of ice-nucleating particle concentrations affects the radiative properties of tropical convective cloud systems, Atmos. Chem. Phys., 21, 5439–5461, https://doi.org/10.5194/acp-21-5439-2021, 2021.

Hiranuma, N., Brooks, S. D., Moffet, R. C., Glen, A., Laskin, A., Gilles, M. K., Liu, P., Macdonald, A. M., Strapp, J. W., and McFarquhar, G. M.: Chemical characterization of individual particles and residuals of cloud droplets and ice crystals collected on board research aircraft in the ISDAC 2008 study, J. Geophys. Res.-Atmos., 118, 6564–6579, https://doi.org/10.1002/jgrd.50484, 2013.

Hoose, C. and Möhler, O.: Heterogeneous ice nucleation on atmospheric aerosols: a review of results from labo-

ratory experiments, Atmos. Chem. Phys., 12, 9817–9854, https://doi.org/10.5194/acp-12-9817-2012, 2012.

Huang, J. and Jaeglé, L.: Wintertime enhancements of sea salt aerosol in polar regions consistent with a sea ice source from blowing snow, Atmos. Chem. Phys., 17, 3699–3712, https://doi.org/10.5194/acp-17-3699-2017, 2017.

Huang, Z., Huang, J., Hayasaka, T., Wang, S., Zhou, T., and Jin, H.: Short-cut transport path for Asian dust directly to the Arctic: a case study, Environ. Res. Lett., 10, 114018, https://doi.org/10.1088/1748-9326/10/11/114018, 2015.

Huneeus, N., Schulz, M., Balkanski, Y., Griesfeller, J., Prospero, J., Kinne, S., Bauer, S., Boucher, O., Chin, M., Dentener, F., Diehl, T., Easter, R., Fillmore, D., Ghan, S., Ginoux, P., Grini, A., Horowitz, L., Koch, D., Krol, M. C., Landing, W., Liu, X., Mahowald, N., Miller, R., Morcrette, J.-J., Myhre, G., Penner, J., Perlwitz, J., Stier, P., Takemura, T., and Zender, C. S.: Global dust model intercomparison in AeroCom phase I, Atmos. Chem. Phys., 11, 7781–7816, https://doi.org/10.5194/acp-11-7781-2011, 2011.

Irish, V. E., Elizondo, P., Chen, J., Chou, C., Charette, J., Lizotte, M., Ladino, L. A., Wilson, T. W., Gosselin, M., Murray, B. J., Polishchuk, E., Abbatt, J. P. D., Miller, L. A., and Bertram, A. K.: Ice-nucleating particles in Canadian Arctic sea-surface microlayer and bulk seawater, Atmos. Chem. Phys., 17, 10583–10595, https://doi.org/10.5194/acp-17-10583-2017, 2017.

Irish, V. E., Hanna, S. J., Willis, M. D., China, S., Thomas, J. L., Wentzell, J. J. B., Cirisan, A., Si, M., Leaitch, W. R., Murphy, J. G., Abbatt, J. P. D., Laskin, A., Girard, E., and Bertram, A. K.: Ice nucleating particles in the marine boundary layer in the Canadian Arctic during summer 2014, Atmos. Chem. Phys., 19, 1027–1039, https://doi.org/10.5194/acp-19-1027-2019, 2019.

Kanji, Z. A., Ladino, L. A., Wex, H., Boose, Y., Burkert-Kohn, M., Cziczo, D. J., and Krämer, M.: Overview of Ice Nucleating Particles, Meteor. Mon., 58, 1.1–1.33, https://doi.org/10.1175/amsmonographs-d-16-0006.1, 2017.

Kirpes, R. M., Bondy, A. L., Bonanno, D., Moffet, R. C., Wang, B., Laskin, A., Ault, A. P., and Pratt, K. A.: Secondary sulfate is internally mixed with sea spray aerosol and organic aerosol in the winter Arctic, Atmos. Chem. Phys., 18, 3937–3949, https://doi.org/10.5194/acp-18-3937-2018, 2018.

Kirpes, R. M., Bonanno, D., May, N. W., Fraund, M., Barget, A. J., Moffet, R. C., Ault, A. P., and Pratt, K. A.: Wintertime Arctic Sea Spray Aerosol Composition Controlled by Sea Ice Lead Microbiology, ACS Cent Sci., 5, 1760–1767, https://doi.org/10.1021/acscentsci.9b00541, 2019.

Kirpes, R. M., Rodriguez, B., Kim, S., China, S., Laskin, A., Park, K., Jung, J., Ault, A. P., and Pratt, K. A.: Emerging investigator series: influence of marine emissions and atmospheric processing on individual particle composition of summertime Arctic aerosol over the Bering Strait and Chukchi Sea, Environ. Sci. Process. Impacts, 22, 1201–1213, https://doi.org/10.1039/c9em00495e, 2020.

Komurcu, M., Storelvmo, T., Tan, I., Lohmann, U., Yun, Y., Penner, J. E., Wang, Y., Liu, X., and Takemura, T.: Intercomparison of the cloud water phase among global climate models, J. Geophys. Res.-Atmos., 119, 3372–3400, https://doi.org/10.1002/2013jd021119, 2014.

Korolev, A., McFarquhar, G., Field, P. R., Franklin, C., Lawson, P., Wang, Z., Williams, E., Abel, S. J., Axisa, D., Borrmann, S., Crosier, J., Fugal, J., Krämer, M., Lohmann, U., Schlenczek, O., Schnaiter, M., and Wendisch, M.: Mixed-Phase Clouds: Progress and Challenges, Meteor. Mon., 58, 5.1–5.50, https://doi.org/10.1175/amsmonographs-d-17-0001.1, 2017.

Lewis, E. and Schwartz, S.: Sea Salt Aerosol Production: Mechanisms, Methods, Measurements and Models – A Critical Review, GMS, 152, 3719, https://doi.org/10.1029/GM152, 2004.

Lindsley, W. G.: Filter Pore Size and Aerosol Sample Collection, NIOSH Manual of Analytical Methods, 1–14, https://www.cdc.gov/niosh/docs/2014-151/pdfs/chapters/chapter-fp.pdf (last access: 9 May 2018), 2016.

Mason, R. H., Si, M., Chou, C., Irish, V. E., Dickie, R., Elizondo, P., Wong, R., Brintnell, M., Elsasser, M., Lassar, W. M., Pierce, K. M., Leaitch, W. R., MacDonald, A. M., Platt, A., Toom-Sauntry, D., Sarda-Estève, R., Schiller, C. L., Suski, K. J., Hill, T. C. J., Abbatt, J. P. D., Huffman, J. A., DeMott, P. J., and Bertram, A. K.: Size-resolved measurements of ice-nucleating particles at six locations in North America and one in Europe, Atmos. Chem. Phys., 16, 1637–1651, https://doi.org/10.5194/acp-16-1637-2016, 2016.

May, N. W., Quinn, P. K., McNamara, S. M., and Pratt, K. A.: Multiyear study of the dependence of sea salt aerosol on wind speed and sea ice conditions in the coastal Arctic, J. Geophys. Res.-Atmos., 121, 9208–9219, https://doi.org/10.1002/2016jd025273, 2016.

McCluskey, C. S., Ovadnevaite, J., Rinaldi, M., Atkinson, J. D., Belosi, F., Ceburnis, D., Marullo, S., Hill, T. C. J., Lohmann, U., Kanji, Z. A., O'Dowd, C., Kreidenweis, S. M., and DeMott, P. J.: Marine and Terrestrial Organic Ice-Nucleating Particles in Pristine Marine to Continentally Influenced Northeast Atlantic Air Masses, J. Geophys. Res.-Atmos., 123, 6196–6212, https://doi.org/10.1029/2017jd028033, 2018.

McCoy, D. T., Tan, I., Hartmann, D. L., Zelinka, M. D., and Storelvmo, T.: On the relationships among cloud cover, mixed-phase partitioning, and planetary albedo in GCMs, J. Adv. Model. Earth Syst., 8, 650–668, https://doi.org/10.1002/2015ms000589, 2016.

McCoy, D. T., Hartmann, D. L., and Zelinka, M. D.: Chapter 9 – Mixed-Phase Cloud Feedbacks, in: Mixed-Phase Clouds, edited by: Andronache, C., Elsevier, 215–236, https://shop.elsevier.com/books/mixed-phase-clouds/andronache/978-0-12-810549-8 (last access: 23 October 2019), 2018.

Meinander, O., Dagsson-Waldhauserova, P., Amosov, P., Aseyeva, E., Atkins, C., Baklanov, A., Baldo, C., Barr, S. L., Barzycka, B., Benning, L. G., Cvetkovic, B., Enchilik, P., Frolov, D., Gassó, S., Kandler, K., Kasimov, N., Kavan, J., King, J., Koroleva, T., Krupskaya, V., Kulmala, M., Kusiak, M., Lappalainen, H. K., Laska, M., Lasne, J., Lewandowski, M., Luks, B., McQuaid, J. B., Moroni, B., Murray, B., Möhler, O., Nawrot, A., Nickovic, S., O'Neill, N. T., Pejanovic, G., Popovicheva, O., Ranjbar, K., Romanias, M., Samonova, O., Sanchez-Marroquin, A., Schepanski, K., Semenkov, I., Sharapova, A., Shevnina, E., Shi, Z., Sofiev, M., Thevenet, F., Thorsteinsson, T., Timofeev, M., Umo, N. S., Uppstu, A., Urupina, D., Varga, G., Werner, T., Arnalds, O., and Vukovic Vimic, A.: Newly identified climatically and environmentally significant high-latitude dust sources, Atmos. Chem. Phys., 22, 11889–11930, https://doi.org/10.5194/acp-22-11889-2022, 2022.

Ménégoz, M., Voldoire, A., Teyssédre, H., Mélia, D. S. y., Peuch, V. H., and Gouttevin, I.: How does the atmospheric variability drive the aerosol residence time in the Arctic region?, Tellus B, 64, 11596, https://doi.org/10.3402/tellusb.v64i0.11596, 2012.

Murray, B. J., O'Sullivan, D., Atkinson, J. D., and Webb, M. E.: Ice nucleation by particles immersed in supercooled cloud droplets, Chem. Soc. Rev., 41, 6519–6554, https://doi.org/10.1039/c2cs35200a, 2012.

Murray, B. J., Carslaw, K. S., and Field, P. R.: Opinion: Cloud-phase climate feedback and the importance of ice-nucleating particles, Atmos. Chem. Phys., 21, 665–679, https://doi.org/10.5194/acp-21-665-2021, 2021.

O'Sullivan, D., Murray, B. J., Malkin, T. L., Whale, T. F., Umo, N. S., Atkinson, J. D., Price, H. C., Baustian, K. J., Browse, J., and Webb, M. E.: Ice nucleation by fertile soil dusts: relative importance of mineral and biogenic components, Atmos. Chem. Phys., 14, 1853–1867, https://doi.org/10.5194/acp-14-1853-2014, 2014.

O'Sullivan, D., Murray, B. J., Ross, J. F., Whale, T. F., Price, H. C., Atkinson, J. D., Umo, N. S., and Webb, M. E.: The relevance of nanoscale biological fragments for ice nucleation in clouds, Sci. Rep., 5, 8082, https://doi.org/10.1038/srep08082, 2015.

Petters, M. D. and Wright, T. P.: Revisiting ice nucleation from precipitation samples, Geophys. Res. Lett., 42, 8758–8766, https://doi.org/10.1002/2015gl065733, 2015.

Porter, G. C. E., Sikora, S. N. F., Adams, M. P., Proske, U., Harrison, A. D., Tarn, M. D., Brooks, I. M., and Murray, B. J.: Resolving the size of ice-nucleating particles with a balloon deployable aerosol sampler: the SHARK, Atmos. Meas. Tech., 13, 2905–2921, https://doi.org/10.5194/amt-13-2905-2020, 2020.

Porter, G. C. E., Adams, M. P., Brooks, I. M., Ickes, L., Karlsson, L., Leck, C., Salter, M. E., Schmale, J., Siegel, K., Sikora, S. N. F., Tarn, M. D., Vüllers, J., Wernli, H., Zieger, P., Zinke, J., and Murray, B. J.: Highly Active Ice-Nucleating Particles at the Summer North Pole, J. Geophys. Res.-Atmos., 127, 28, https://doi.org/10.1029/2021jd036059, 2022.

Prenni, A. J., Harrington, J. Y., Tjernström, M., DeMott, P. J., Avramov, A., Long, C. N., Kreidenweis, S. M., Olsson, P. Q., and Verlinde, J.: Can Ice-Nucleating Aerosols Affect Arctic Seasonal Climate?, B. Am. Meteorol. Soc., 88, 541–550, https://doi.org/10.1175/bams-88-4-541, 2007.

Prenni, A. J., Demott, P. J., Rogers, D. C., Kreidenweis, S. M., McFarquhar, G. M., Zhang, G., and Poellot, M. R.: Ice nuclei characteristics from M-PACE and their relation to ice formation in clouds, Tellus B, 61, 436–448, https://doi.org/10.1111/j.1600-0889.2009.00415.x, 2009.

Price, H. C., Baustian, K. J., McQuaid, J. B., Blyth, A., Bower, K. N., Choularton, T., Cotton, R. J., Cui, Z., Field, P. R., Gallagher, M., Hawker, R., Merrington, A., Miltenberger, A., Neely Iii, R. R., Parker, S. T., Rosenberg, P. D., Taylor, J. W., Trembath, J., Vergara-Temprado, J., Whale, T. F., Wilson, T. W., Young, G., and Murray, B. J.: Atmospheric Ice-Nucleating Particles in the Dusty Tropical Atlantic, J. Geophys. Res.-Atmos., 123, 2175–2193, https://doi.org/10.1002/2017jd027560, 2018.

Reicher, N., Segev, L., and Rudich, Y.: The WeIzmann Supercooled Droplets Observation on a Microarray (WISDOM) and application for ambient dust, Atmos. Meas. Tech., 11, 233–248, https://doi.org/10.5194/amt-11-233-2018, 2018.

Rinaldi, M., Hiranuma, N., Santachiara, G., Mazzola, M., Mansour, K., Paglione, M., Rodriguez, C. A., Traversi, R., Becagli, S., Cappelletti, D., and Belosi, F.: Ice-nucleating particle concentration measurements from Ny-Ålesund during the Arctic spring–summer in 2018, Atmos. Chem. Phys., 21, 14725–14748, https://doi.org/10.5194/acp-21-14725-2021, 2021.

Rogers, D. C., DeMott, P. J., and Kreidenweis, S. M.: Airborne measurements of tropospheric ice-nucleating aerosol particles in the Arctic spring, J. Geophys. Res.-Atmos., 106, 15053–15063, https://doi.org/10.1029/2000jd900790, 2001.

Rolph, G., Stein, A., and Stunder, B.: Real-time Environmental Applications and Display sYstem: READY, Environ. Model. Software, 95, 210–228, https://doi.org/10.1016/j.envsoft.2017.06.025, 2017.

Rosenberg, P. D., Dean, A. R., Williams, P. I., Dorsey, J. R., Minikin, A., Pickering, M. A., and Petzold, A.: Particle sizing calibration with refractive index correction for light scattering optical particle counters and impacts upon PCASP and CDP data collected during the Fennec campaign, Atmos. Meas. Tech., 5, 1147–1163, https://doi.org/10.5194/amt-5-1147-2012, 2012.

Ryder, C. L., Marenco, F., Brooke, J. K., Estelles, V., Cotton, R., Formenti, P., McQuaid, J. B., Price, H. C., Liu, D., Ausset, P., Rosenberg, P. D., Taylor, J. W., Choularton, T., Bower, K., Coe, H., Gallagher, M., Crosier, J., Lloyd, G., Highwood, E. J., and Murray, B. J.: Coarse-mode mineral dust size distributions, composition and optical properties from AER-D aircraft measurements over the tropical eastern Atlantic, Atmos. Chem. Phys., 18, 17225–17257, https://doi.org/10.5194/acp-18-17225-2018, 2018.

Sanchez-Marroquin, A. and Murray, B. J.: Data for "Aircraft ice-nucleating particle and aerosol composition measurements in the western North American Arctic", University of Leeds [data set], https://doi.org/10.5518/1401, 2023.

Sanchez-Marroquin, A., Hedges, D. H. P., Hiscock, M., Parker, S. T., Rosenberg, P. D., Trembath, J., Walshaw, R., Burke, I. T., McQuaid, J. B., and Murray, B. J.: Characterisation of the filter inlet system on the FAAM BAe-146 research aircraft and its use for size-resolved aerosol composition measurements, Atmos. Meas. Tech., 12, 5741–5763, https://doi.org/10.5194/amt-12-5741-2019, 2019.

Sanchez-Marroquin, A., Arnalds, O., Baustian-Dorsi, K. J., Browse, J., Dagsson-Waldhauserova, P., Harrison, A. D., Maters, E. C., Pringle, K. J., Vergara-Temprado, J., Burke, I. T., McQuaid, J. B., Carslaw, K. S., and Murray, B. J.: Iceland is an episodic source of atmospheric ice-nucleating particles relevant for mixed-phase clouds, Sci. Adv., 6, eaba8137, https://doi.org/10.1126/sciadv.aba8137, 2020.

Sanchez-Marroquin, A., West, L. S., Burke, I. T., McQuaid, J. B., and Murray, B. J.: Mineral and biological ice-nucleating particles above the South East of the British Isles, Environ. Sci.-Atmos., 2021, 176–191, https://doi.org/10.1039/D1EA00003A, 2021.

Santl-Temkiv, T., Lange, R., Beddows, D., Rauter, U., Pilgaard, S., Dall'Osto, M., Gunde-Cimerman, N., Massling, A., and Wex, H.: Biogenic Sources of Ice Nucleating Particles at the High Arctic Site Villum Research Station, Environ. Sci. Technol., 53, 10580–10590, https://doi.org/10.1021/acs.est.9b00991, 2019.

Schnell, R. C.: Airborne ice nucleus measurements around the Hawaiian Islands, J. Geophys. Res., 87, 8886, https://doi.org/10.1029/JC087iC11p08886, 1982.

Shi, Y., Liu, X., Wu, M., Zhao, X., Ke, Z., and Brown, H.: Relative importance of high-latitude local and long-range-transported dust for Arctic ice-nucleating particles and impacts on Arctic mixed-phase clouds, Atmos. Chem. Phys, 22, 2909-2935,https://doi.org/10.5194/acp-22-2909-2022, 2022.

Si, M., Evoy, E., Yun, J., Xi, Y., Hanna, S. J., Chivulescu, A., Rawlings, K., Veber, D., Platt, A., Kunkel, D., Hoor, P., Sharma, S., Leaitch, W. R., and Bertram, A. K.: Concentrations, composition, and sources of ice-nucleating particles in the Canadian High Arctic during spring 2016, Atmos. Chem. Phys., 19, 3007–3024, https://doi.org/10.5194/acp-19-3007-2019, 2019.

Soo, J. C., Monaghan, K., Lee, T., Kashon, M., and Harper, M.: Air sampling filtration media: Collection efficiency for respirable size-selective sampling, Aerosol Sci. Technol., 50, 76–87, https://doi.org/10.1080/02786826.2015.1128525, 2016.

Stein, A. F., Draxler, R. R., Rolph, G. D., Stunder, B. J. B., Cohen, M. D., and Ngan, F.: NOAA's HYSPLIT Atmospheric Transport and Dispersion Modeling System, B. Am. Meteorol. Soc., 96, 2059–2077, https://doi.org/10.1175/bams-d-14-00110.1, 2015.

Storelvmo, T., Tan, I., and Korolev, A. V.: Cloud Phase Changes Induced by CO_2 Warming – a Powerful yet Poorly Constrained Cloud-Climate Feedback, Current Climate Change Reports, 1, 288–296, https://doi.org/10.1007/s40641-015-0026-2, 2015.

Tan, I., Storelvmo, T., and Zelinka, M. D.: Observational constraints on mixed-phase clouds imply higher climate sensitivity, Science, 352, 224–227, https://doi.org/10.1126/science.aad5300, 2016.

Tobo, Y., Adachi, K., DeMott, P. J., Hill, T. C. J., Hamilton, D. S., Mahowald, N. M., Nagatsuka, N., Ohata, S., Uetake, J., Kondo, Y., and Koike, M.: Glacially sourced dust as a potentially significant source of ice nucleating particles, Nat. Geosci., 12, 253-+, https://doi.org/10.1038/s41561-019-0314-x, 2019.

Ullrich, R., Hoose, C., Mohler, O., Niemand, M., Wagner, R., Hohler, K., Hiranuma, N., Saathoff, H., and Leisner, T.: A New Ice Nucleation Active Site Parameterization for Desert Dust and Soot, J. Atmos. Sci., 74, 699–717, https://doi.org/10.1175/Jas-D-16-0074.1, 2017.

Vali, G.: Quantitative Evaluation of Experimental Results an the Heterogeneous Freezing Nucleation of Supercooled Liquids, J. Atmos. Sci., 28, 402–409, https://doi.org/10.1175/1520-0469(1971)028<0402:QEOERA>2.0.CO;2, 1971.

Vali, G.: Revisiting the differential freezing nucleus spectra derived from drop-freezing experiments: methods of calculation, applications, and confidence limits, Atmos. Meas. Tech., 12, 1219–1231, https://doi.org/10.5194/amt-12-1219-2019, 2019.

VanCuren, R. A., Cahill, T., Burkhart, J., Barnes, D., Zhao, Y., Perry, K., Cliff, S., and McConnell, J.: Aerosols and their sources at Summit Greenland – First results of continuous size- and time-resolved sampling, Atmos. Environ., 52, 82–97, https://doi.org/10.1016/j.atmosenv.2011.10.047, 2012.

Vergara-Temprado, J., Murray, B. J., Wilson, T. W., O'Sullivan, D., Browse, J., Pringle, K. J., Ardon-Dryer, K., Bertram, A. K., Burrows, S. M., Ceburnis, D., DeMott, P. J., Mason, R. H., O'Dowd, C. D., Rinaldi, M., and Carslaw, K. S.: Contribution of feldspar and marine organic aerosols to global ice nucleating particle concentrations, Atmos. Chem. Phys., 17, 3637–3658, https://doi.org/10.5194/acp-17-3637-2017, 2017.

Vergara-Temprado, J., Miltenberger, A. K., Furtado, K., Grosvenor, D. P., Shipway, B. J., Hill, A. A., Wilkinson, J. M., Field, P. R., Murray, B. J., and Carslaw, K. S.: Strong control of Southern Ocean cloud reflectivity by ice-nucleating particles, P. Natl. Acad. Sci. USA, 115, 2687–2692, https://doi.org/10.1073/pnas.1721627115, 2018.

Welti, A., Bigg, E. K., DeMott, P. J., Gong, X., Hartmann, M., Harvey, M., Henning, S., Herenz, P., Hill, T. C. J., Hornblow, B., Leck, C., Löffler, M., McCluskey, C. S., Rauker, A. M., Schmale, J., Tatzelt, C., van Pinxteren, M., and Stratmann, F.: Ship-based measurements of ice nuclei concentrations over the Arctic, Atlantic, Pacific and Southern oceans, Atmos. Chem. Phys., 20, 15191–15206, https://doi.org/10.5194/acp-20-15191-2020, 2020.

Wex, H., Huang, L., Zhang, W., Hung, H., Traversi, R., Becagli, S., Sheesley, R. J., Moffett, C. E., Barrett, T. E., Bossi, R., Skov, H., Hünerbein, A., Lubitz, J., Löffler, M., Linke, O., Hartmann, M., Herenz, P., and Stratmann, F.: Annual variability of ice-nucleating particle concentrations at different Arctic locations, Atmos. Chem. Phys., 19, 5293–5311, https://doi.org/10.5194/acp-19-5293-2019, 2019.

Whale, T. F., Murray, B. J., O'Sullivan, D., Wilson, T. W., Umo, N. S., Baustian, K. J., Atkinson, J. D., Workneh, D. A., and Morris, G. J.: A technique for quantifying heterogeneous ice nucleation in microlitre supercooled water droplets, Atmos. Meas. Tech., 8, 2437–2447, https://doi.org/10.5194/amt-8-2437-2015, 2015.

Wilson, T. W., Ladino, L. A., Alpert, P. A., Breckels, M. N., Brooks, I. M., Browse, J., Burrows, S. M., Carslaw, K. S., Huffman, J. A., Judd, C., Kilthau, W. P., Mason, R. H., McFiggans, G., Miller, L. A., Najera, J. J., Polishchuk, E., Rae, S., Schiller, C. L., Si, M., Vergara-Temprado, J., Whale, T. F., Wong, J. P., Wurl, O., Yakobi-Hancock, J. D., Abbatt, J. P., Aller, J. Y., Bertram, A. K., Knopf, D. A., and Murray, B. J.: A marine biogenic source of atmospheric ice-nucleating particles, Nature, 525, 234–238, https://doi.org/10.1038/nature14986, 2015.

Yang, X., Pyle, J. A., and Cox, R. A.: Sea salt aerosol production and bromine release: Role of snow on sea ice, Geophys. Res. Lett., 35, 1–5, https://doi.org/10.1029/2008gl034536, 2008.

Young, G., Jones, H. M., Darbyshire, E., Baustian, K. J., McQuaid, J. B., Bower, K. N., Connolly, P. J., Gallagher, M. W., and Choularton, T. W.: Size-segregated compositional analysis of aerosol particles collected in the European Arctic during the ACCACIA campaign, Atmos. Chem. Phys., 16, 4063–4079, https://doi.org/10.5194/acp-16-4063-2016, 2016.

Yun, J., Evoy, E., Worthy, S. E., Fraser, M., Veber, D., Platt, A., Rawlings, K., Sharma, S., Leaitch, W. R., and Bertram, A.: Ice nucleating particles in the Canadian High Arctic during the fall of 2018, Environ. Sci.-Atmos., 2, 279–290, https://doi.org/10.1039/d1ea00068c, 2022.

Zhao, X., Huang, K., Fu, J. S., and Abdullaev, S. F.: Long-range transport of Asian dust to the Arctic: identification of transport pathways, evolution of aerosol optical properties, and impact assessment on surface albedo changes, Atmos. Chem. Phys., 22, 10389–10407, https://doi.org/10.5194/acp-22-10389-2022, 2022.